Nano Energy 41 (2017) 772–779

Contents lists available at ScienceDirect

Nano Energy

journal homepage: www.elsevier.com/locate/nanoen

Full paper

Co-N-doped MoO_2 nanowires as efficient electrocatalysts for the oxygen reduction reaction and hydrogen evolution reaction

Linjing Yang[a], Jiayuan Yu[a], Zhaoqian Wei[a], Guixiang Li[a], Lindie Cao[a], Weijia Zhou[a,*], Shaowei Chen[a,b,**]

[a] New Energy Research Institute, Guangdong Provincial Key Laboratory of Atmospheric Environment and Pollution Control, School of Environment and Energy, South China University of Technology, Guangzhou Higher Education Mega Center, Guangzhou, Guangdong 510006, China
[b] Department of Chemistry and Biochemistry, University of California, 1156 High Street, Santa Cruz, CA 95064, United States

ARTICLE INFO

Keywords:
MoO_2 nanowires
Templates
Doping
Oxygen reduction reaction
Hydrogen evolution reaction

ABSTRACT

Oxygen reduction reaction (ORR) and hydrogen evolution reaction (HER) are traditionally carried out with noble metals (such as Pt) as catalysts, respectively. Herein, Co-N-doped MoO_2 nanowires catalysts were synthesized by employing MoO_2 nanowires as templates and conductive substrates. The effect of nanowire structure and non-metal/metal doping on ORR and HER performance were scientific discussed. The most active Co-N-MoO_2 (Co-N-doped MoO_2) exhibited high ORR catalytic activity (an onset potential of +0.87 V vs. RHE, n values of 3.56 and 3.68, excellent electrochemical stability) and outstanding HER performance with a low overpotential (69 mV vs. RHE), high electrochemical area and robust stability in 0.1 M KOH, which are associated with the defined nanowires structure, and homogeneous doping of Co/N into MoO_2 with numerous active sites.

1. Introduction

The development of oxygen reduction reactions (ORR) electrocatalysts with efficient activity and robust stability is crucial to solve the energy shortage problems, which plays key roles in proton exchange membrane fuel cells and zinc-air batteries, and so on. Meantime, hydrogen evolution reaction (HER) is significant in the production of pollution-free and sustainable energy. Platinum-based noble materials have been known as the best electrocatalysts with excellent ORR and HER catalytic activity [1,2]. However, their widespread applications in ORR or HER are restricted because of high cost and low abundance. Thus, one of critical challenges is exploring low-cost, non-noble metal efficient electrocatalysts for ORR and HER [3,4].

In fact, extensive efforts have been contributed to alternative materials of low costs and rich earth abundance that may eventually replace platinum-based catalysts [5,6]. A variety of materials, including carbon nanostructures [7–9], transition metals [10–12] and their oxides [13–15], carbides [7,16], and disulfides [17,18] have been prepared and examined as electrocatalysts for ORR or HER. It is worth noting that molybdenum dioxide (MoO_2) with a rutile structure possess metallic properties with an electrical resistivity of 8.8×10^{-5} Ω cm at 300 K and high chemical stability [19,20]. Prof. Shen and Prof. Cui reported the porous MoO_2 nanosheets grown on Ni foam by the wet-chemical route and followed annealing possessed high performance for HER and OER, which attributed to porous nanostructure and good conductivity [21].

In addition, extensive work about the heteroatom doped electrocatalysts, such as N, P, S, Fe or Co has been reported, which exhibited an enhanced ORR and HER performance due to their unique electronic properties [22–25]. For example, Prof. Guo reported that cobalt and nitrogen co-embedded in mesoporous carbon significantly promoted electron penetration to enhance the ORR catalytic activity, which is attributed to the homogeneous distribution of abundant Co-N actives sites on the surface of the mesoporous carbon [16]. Our group also reported N-doped carbon coated Co nanoparticles onto N doped graphene substrates possessed the efficient HER electrocatalytic activity (small overpotential of 49 mV and Tafel slope is 79.3 mV dec^{-1}) due to the promotion of cobalt nanoparticles entrapped into carbon shell [26,27]. However, the other conductive substrates, such as MoO_2, as active catalysts enhanced by the optimized selection of N/Co doping need breakthroughs.

Recently, we demonstrated that MoO_2 nanowires can be employed

* Corresponding author.
** Corresponding author at: New Energy Research Institute, Guangdong Provincial Key Laboratory of Atmospheric Environment and Pollution Control, School of Environment and Energy, South China University of Technology, Guangzhou Higher Education Mega Center, Guangzhou, Guangdong 510006, China.
E-mail addresses: eszhouwj@scut.edu.cn (W. Zhou), shaowei@ucsc.edu (S. Chen).

http://dx.doi.org/10.1016/j.nanoen.2017.03.032
Received 29 January 2017; Received in revised form 14 March 2017; Accepted 16 March 2017
Available online 18 March 2017
2211-2855/

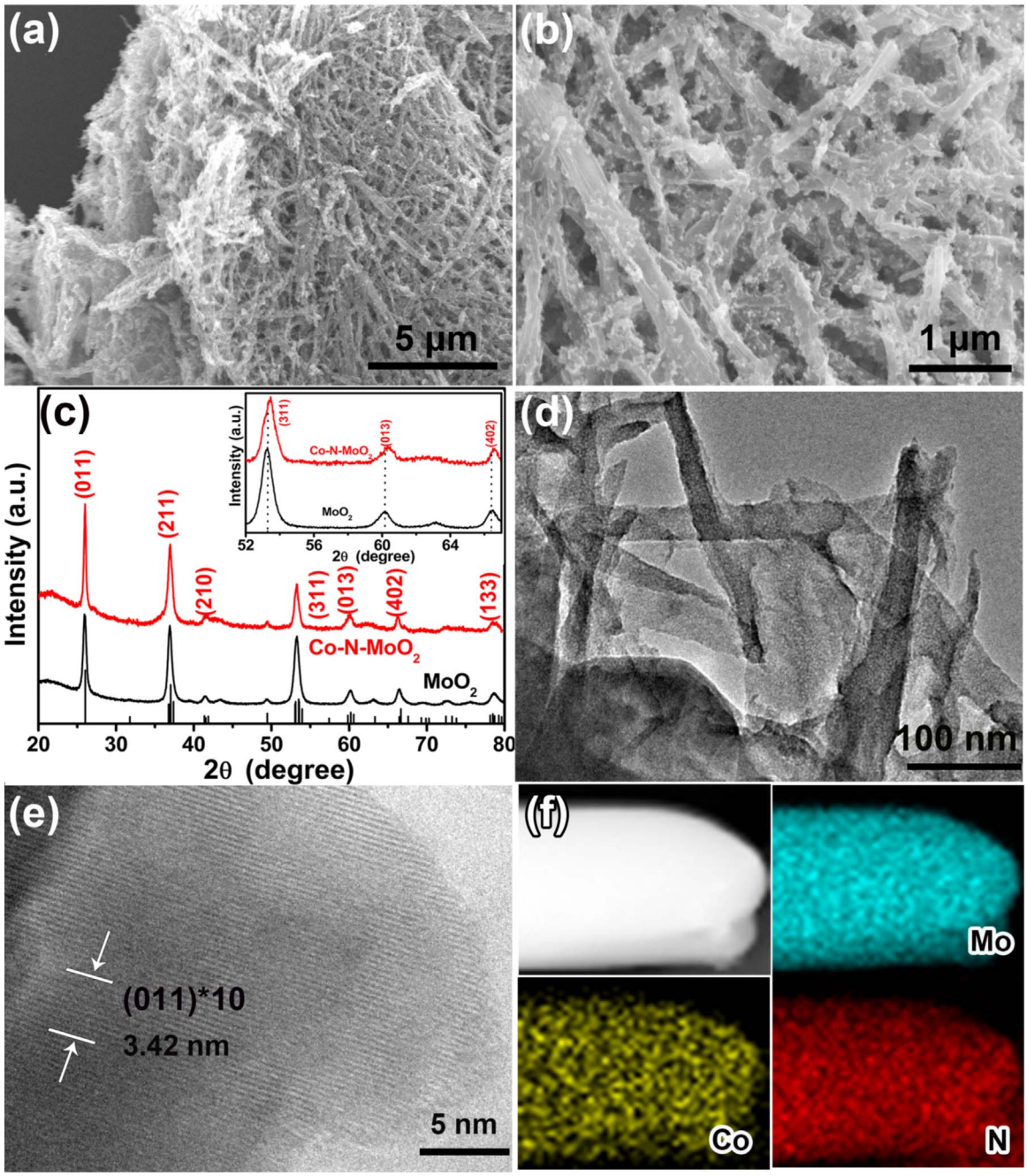

Fig. 1. SEM images (a, b), XRD patterns and the corresponding zoom-in regions (inset) (c), (HR)TEM images (d, e), elements mapping for Mo, Co, N (f) of Co-N-MoO_2.

as nanowire templates and conductive substrates for ORR and HER. The deliberate doping with N and Co atoms into MoO_2 nanowires as bifunctional electrocatalysts enhanced the ORR and HER catalytic activity. The obtained Co-N-MoO_2 catalysts exhibited high activities and long-term durability towards ORR and HER in alkaline electrolyte (0.1 M KOH), which are associated with the defined nanowire structures, and homogeneous doping of Co/N into MoO_2 with numerous active sites.

2. Experimental

2.1. Preparation of Cobalt and Nitrogen Co-Doped MoO_2 nanowires (Co-N-doped MoO_2)

First, the molybdenum dioxide nanowires (MoO_2 NWs) were prepared according to the reported method with modifications [28]. Second, 255.9 mg of the obtained MoO_2 NWs and 59.78 mg Bis(acetylacetonato)cobalt ($Co(C_5H_7O_2)_3$) were added into 30 mL DI-water to form a mixture. The reaction was stirred for 10 h at 80 °C. After that, the reaction mixture was transferred to a 40 mL autoclave for hydrothermal reaction at 150 °C for 3 h. The resulted Co doped MoO_2 nanowires were collected by centrifugation and washed with ethanol. At last, 50 mg of the prepared Co doped MoO_2 nanowires and 20 mg of dicyanamide ($C_2H_4N_4$) were dispersed into 20 mL of ethanol under continuous stirring. After the drying, the obtained products were heated at 450 °C for 1 h, then 650 °C for 2 h under an argon atmosphere. The above products were further treated by 1.0 M HCl to remove excess Co compounds, and the Co-N-MoO_2 nanowires were finally obtained. In addition, N-doped MoO_2 nanowires were prepared by similar process without adding $Co(C_5H_7O_2)_3$ as blank samples.

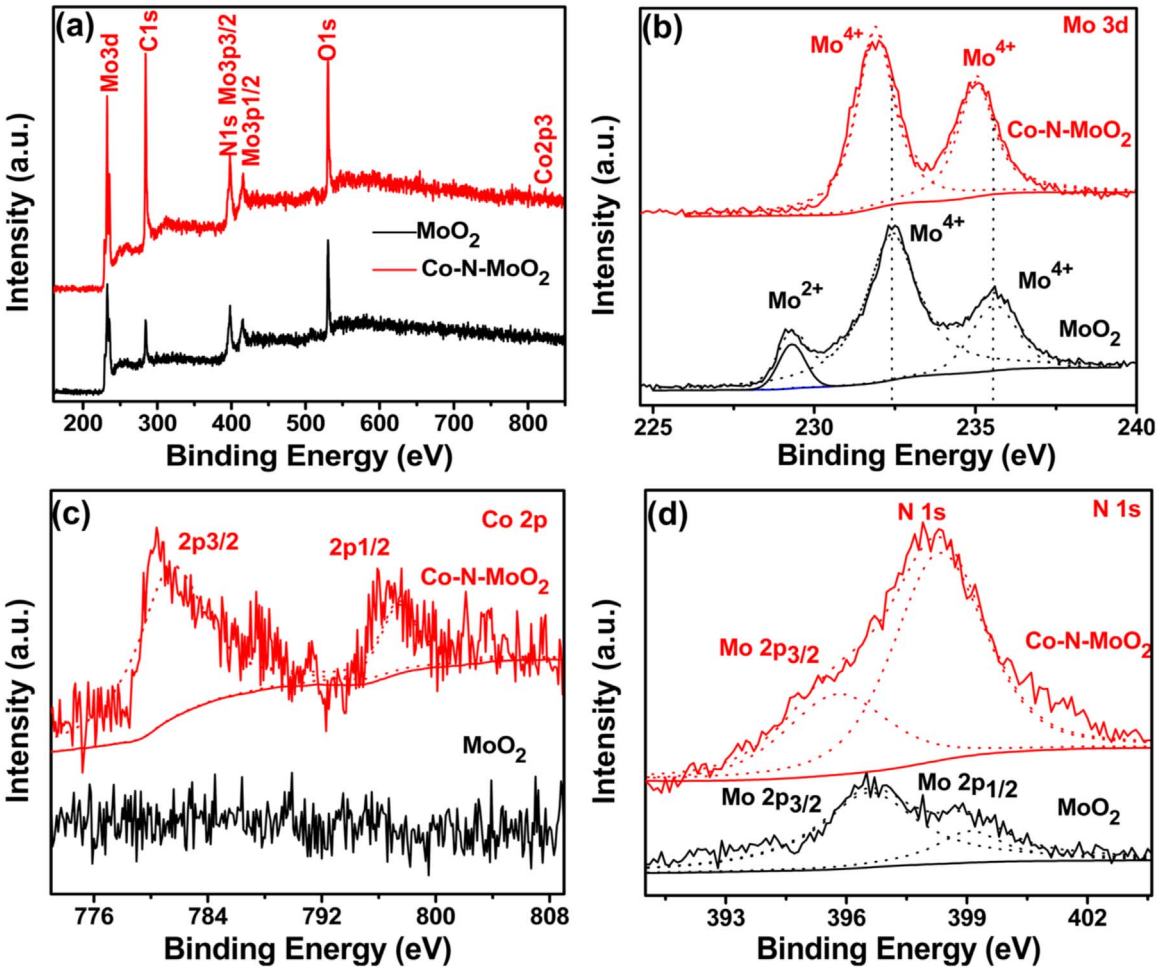

Fig. 2. XPS survey spectra of pure MoO_2 and Co-N-MoO_2 (a) and high-resolution scan of the Mo 3d (b), Co 2p (c) and N 1s (d) electrons.

2.2. Characterization

Field-emission scanning electron microscopic (FESEM, NOVA NANOSEM 430, FEI) and Transmission electron microscopic (TEM, Tecnai G220 FEI) measurements were employed to characterize the morphologies and structures of the as-prepared electrocatalysts. Powder X-ray diffraction (XRD, Bruker D8 Advance powder X-ray diffractometer, Cu Kα (λ=0.15406 nm)), and X-ray photoelectron spectroscopic (XPS, PHI X-tool instrument) were carried out to characterize the crystal structure, elementary composition. Nitrogen adsorption-desorption analysis was conducted with an ASAP 2020 instrument to evaluate the specific surface areas of the samples.

2.3. Electrochemistry

Electrochemical measurements of ORR and HER activity were performed with a CHI 750E electrochemical workstation (CH Instruments Inc.) in 0.1 M KOH aqueous solution. A rotating ring-disk electrode (RRDE) with a glassy carbon disk and gold ring was used as the working electrode. A Hg/Hg_2Cl_2 electrode and a carbon rod were used as the reference and counter electrode, respectively. 4 mg of the catalyst powders was dispersed in 1 mL of 1:4 (v:v) ethanol/water mixed solvents along with 80 μL of a Nafion solution (5% Nafion in ethanol), and the mixture was sonicated for 30 min. Then, 10 μL of the above solution was dropcast onto the surface of the RRDE at the catalyst loading of 0.204 mg cm^{-2} and dried at room temperature. For ORR, the polarization curves were acquired at 10 mV s^{-1} from 0 to −1.0 V (vs. SCE) at different electrode rotation rates (400–2025 rpm) at O_2-saturated 0.1 M KOH. CV tests were performed at 50 mV s^{-1} from 0 to −1.0 V (vs. SCE) in N_2 and O_2-saturated 0.1 M KOH. The numbers of electron transfer were calculated from RRDE data using the equation, $n = 4I_D/(I_D + I_R/N)$, where I_D and I_R are the disk current and the ring current, respectively, and N is the current collection efficiency (0.37) of the Au ring. Chronoamperometric measurements were performed at +0.47 V vs. RHE for 10 h in O_2-saturated 0.1 M KOH. For HER, polarization curves were acquired by sweeping electrode potentials from −0.8 to −1.6 V (vs. SCE) at a potential sweep rate of 5 mV s^{-1}. Accelerated stability tests were performed at room temperature by potential cycling between −0.8 and −1.4 V (vs. SCE) at a sweep rate of 100 mV s^{-1} for 1000 cycles. Current-time responses were monitored by chronoamperometric measurements at −0.32 V vs. RHE for 10 h.

3. Results and discussion

The morphology and the structure of the prepared Co-N-MoO_2 were examined by scanning electron microscopy (SEM). From Fig. 1a and b, Co-N-MoO_2 possessed the nanowire morphology with nanoparticles on the surface, which inherited the morphology of MoO_2 (Fig. S1 in the Supporting Information). After Co and N doping, there is no obvious morphology change between Co-N-MoO_2 and MoO_2. Fig. 1c showed the XRD patterns of MoO_2 and Co-N-MoO_2. All the diffraction peaks at 26°, 36.98°, 41.62°, 53.46°, 60.32°, 66.5°, 78.8° (black curve) can be indexed to the (011), (211), (210), (311), (013), (402), (133) of crystal faces for the monoclinic MoO_2 (JCPDS number. 32-0671) [29]. After Co and N doping, the diffraction peaks of MoO_2 did not change obviously (red curve). Meanwhile, the XRD patterns in Co-N-MoO_2 show a slight shift to higher diffraction angle in comparison with pure

MoO_2. In inset of Fig. 1c, after doping Co, N into bare MoO_2, (311), (013) and (402) planes of Co-N-MoO_2 shift to the higher angles. The smaller Co atoms substituted for Mo atoms randomly in the crystal structure, then facilitated the shrink of MoO_2 unit cell, implying the successful Co doping into MoO_2. This observation is consistent with the Co or Fe-doped Mo_2C [30,31]. In addition, the N and O atoms possessed the similar atomic radius, and N doping caused the ignored lattice distortion. TEM measurements were then performed to further characterize the morphology and structure of the Co-N-MoO_2 catalysts. Fig. 1d showed that Co-N-MoO_2 exhibited the nanowire morphology with width of 30–40 nm and length of 0.2–0.3 μm. The HRTEM image in Fig. 1e clearly showed the very well-defined lattice fringes with an interplanar spacing of 0.342 nm that was in good agreement with the (011) crystal faces of MoO_2. No other crystal lattices of impureness were observed. The elements mapping (Fig. 1f) confirmed the presence of Mo, Co, and N with uniform wire-like distribution in the Co-N-MoO_2 product, implying the successful Co and N doping into MoO_2. In addition, the BET specific surface area of MoO_2 and Co-N-MoO_2 measured the N_2 adsorption-desorption method have the values of 23.82 $m^2 g^{-1}$ and 31.97 $m^2 g^{-1}$, respectively (Fig. S2**)**. The pore volume of 0.19 $cm^3 g^{-1}$ with a pore size distribution of 4–10 nm for Co-N-MoO_2 was obtained. The above results confirmed the MoO_2 nanowire is a potential substrate for catalysis due to the defined nanowire structure with porous structure.

Elemental characteristics of pure MoO_2 and Co-N-MoO_2 were further studied by XPS measurement with full spectra (Fig. 2a) and high-resolution spectra for Mo (Fig. 2b), Co (Fig. 2c) and N (Fig. 2d). The binding energies of Mo^{4+}3d 5/2 and Mo^{4+}3d 3/2 for Co-N-MoO_2 (red curve, Fig. 2b) can be found at 231.9 and 235 eV, compared with those of bare MoO_2 (Mo^{4+}3d 5/2 232.4 eV, Mo^{4+}3d 3/2 235.5 eV and Mo^{2+}229.3 eV, black curve) [32]. The negative shift of 0.5 eV suggested that electron transfer possibly took place from the MoO_2 nanowires into the doping N and Co. The binding energies of Co 2p3/2 and Co 2p1/2 for Co-N-MoO_2 (red curve, Fig. 2c) can be identified at 782.3 and 796.9 eV, in comparison with those of pure MoO_2 (without any distinct peaks, black curve), suggesting the successful Co doping into MoO_2 nanowires. For the high resolution XPS spectrum of N 1s (Fig. 2d), it was complicated that peak of N 1s was partially overlapped with the Mo 2p1/2 peak at ~395 eV [33–35]. The MoO_2 nanowires detected Mo 2p3/2 at 396.5 eV and Mo 2p1/2 at 398.9 eV. The peak intensity of Mo 2p3/2 was higher than that of Mo 2p1/2, and the intensity ratio was about 1.13. After the calcination of MoO_2 nanowires by $Co(C_5H_7O_2)_3$ and dicyanamide, the apparent peak of N 1s at 398.3 eV appeared and caused the decreased intensity ratio of about 0.71 between peak at 396.5 eV and peak at 398.9 eV, suggesting successful N doping into MoO_2 nanowires. Furthermore, on the basis of the integrated peak areas, the atomic contents of Co and N in Co-N-MoO_2 were estimated to be 2.1 at% and 4.32 at%, respectively. The atomic contents of Co and N of Co-N-MoO_2 nanowires synthesized with various amount of $Co(C_5H_7O_2)_3$ and $C_2H_4N_4$ were shown in Fig. S3 and summarized in Table S1.

The electrocatalytic activities of the Co-N-MoO_2 and a series of control samples including MoO_2, N-MoO_2, Co-MoO_2, and 20 wt% Pt/C were then investigated. As shown in Fig. S4**,** the rotating ring-disk electrode (RRDE) voltammograms of Co-N-MoO_2 suggested that the Co-N-MoO_2 is the multifunctional electrocatalysts for ORR and HER in 0.1 M KOH solution. Fig. S5a and S5c depicted the RRDE voltammograms for the four samples prepared by different amount of $Co(C_5H_7O_2)_3$ and dicyanamide. As depicted in Fig. S6, cyclic voltammetric measurements of Co-N-MoO_2 tested in O_2 saturated 0.1 M KOH showed the apparent cathodic current emerged at approximately +0.87 V. Whereas, only a double-layer charging current was seen in N_2-saturated electrolyte. As shown in Fig. 3a, MoO_2 NWs (TEM image shown in Fig. S7) possess the poor ORR activity by itself with the onset potential at +0.78 V vs RHE. When chemically doped with Co and N, Co-N-MoO_2 exhibits surprisingly high ORR performance with an onset potential of +0.87 V vs. RHE, comparable to that of 20 wt% Pt/C (+0.95 V), and a higher diffusion limited current density (5.39 mA cm^{-2} at +0.4 V) than that of 20 wt% Pt/C (5.11 mA cm^{-2}). In order to study the ORR mechanism of Co-N-MoO_2, the similar slope of Co-N-MoO_2 (60 mV dec^{-1}) with Pt/C (63 mV dec^{-1}) indicated that the rate-determining step both of them was the first electron reduction of oxygen (Fig. S8). The fact that the onset potential of Co-N-MoO_2 was markedly more positive than that of Co-MoO_2 (+0.84 V vs. RHE), N-MoO_2 (+0.81 V vs. RHE) signifies the important role of the Co and N co-doped in enhancing the ORR activity of MoO_2 due to a synergistic interaction between the MoO_2 and the Co/N doping.

RRDE measurements at different rotation rates (from 400 to 2025 rpm) were also carried out to further investigate the electron-transfer kinetics of Co-N-MoO_2, and the results are shown in Fig. 3b. The Koutecky–Levich (K-L) plots within the potential range of +0.55 V to +0.67 V are included in Fig. S9. The good linearity with a consistent slope of Co-N-MoO_2 suggests first-order reaction kinetics, with respect to oxygen concentration in the electrolyte. The difference in ORR performance is also obvious in the number of electron transfers (n). As depicted in Fig. 3c**,** the n values for Co-N-MoO_2 were between 3.56 and 3.68 within the potential range of 0 to +0.8 V, signifying that ORR largely followed a four-electron pathway, similar with 20 wt% Pt/C (3.92–3.78). In contrast, the n values for Co-MoO_2, N-MoO_2 and MoO_2 were significantly lower, at only 1.06–3.72, 2.64–3.63 and 1.34–2.86, respectively. The high electrocatalytic activity of Co-N-MoO_2 was also confirmed by the H_2O_2 percent yield during the ORR, which was < 10% in the low overpotential range from +0.50 to +0.70 V (Fig. S10).

As shown in Fig. 3d, the durability of Co-N-MoO_2 was tested by chronoamperometric measurements. It can be seen that, in addition to a high activity, Co-N-MoO_2 also exhibited robust stability in an O_2-saturated 0.1 M KOH solution. After continuous operation at +0.47 V for 10 h, ~97.01% of the current density was remained, but only 84.05% for commercial 20 wt% Pt/C. In addition, after the injection of 1 M methanol into the electrolyte, the 20 wt% Pt/C showed a highly reduced current density due to CO poisoning from oxidation of methanol (inset of Fig. 3d). In contrast, the ORR currents of Co-N-MoO_2 remained virtually unchanged, confirming the strong tolerance to methanol crossover. Significantly, the Co-N-MoO_2 with high catalytic activity is comparable to or even smaller than those of many metal compound-based ORR catalysts, such as $Co_{0.50}Mo_{0.50}O_yN_z$ (onset potential +0.80 V) [36], $Co_3Mo_2O_xN_{6-x}$/C (onset potential +0.90 V) [37], Co_3O_4/N doped-reduced grapheme oxide (onset potential +0.90 V) [38], cobalt-nitrogen-graphene (onset potential +0.87 V, n=3.44–3.72) [39], and yolk-shell cobalt-nitrogen co-doped porous carbon (onset potential +0.94 V, n=3.5) [40] (Table S2).

The polarization curves for the four samples prepared by different amount of $Co(C_5H_7O_2)_3$ and dicyanamide as shown in Fig. S5b and S5d. The HER electrocatalytic activities of Co-N-MoO_2 including the contrast samples of MoO_2, N-MoO_2, Co-MoO_2 and 20 wt% Pt/C were tested in a three-electrode system in 0.1 M KOH. As shown in Fig. 4a, the onset potential of Co-N-MoO_2 was −69 mV vs. RHE (1 mA cm^{-2}), which was markedly better than that of MoO_2 (−280 mV vs. RHE), N-MoO_2 (−212 mV vs. RHE) and Co-MoO_2 (−158 mV vs. RHE). The results confirmed that the synergetic effect between doped N and doped Co played a vital role in enhancing HER activity of Co-N-MoO_2. However, the onset potential of Co-N-MoO_2 was still inferior to that of 20 wt% Pt/C (−8 mV vs. RHE). Additional, for Co-N-MoO_2, the overpotentials need to drive cathodic current densities of 10 and 20 mA cm^{-2} were 258 and 336 mV, respectively. Tafel slopes revealed the inherent reaction processes of the HER (Fig. 4b). The Tafel slope of 20 wt% Pt/C was 38.9 mV dec^{-1}, consistent with published literatures in 0.1 M KOH [41]. In contrast, Co-N-MoO_2 possessed a Tafel slope of 126.8 mV dec^{-1}, lower than that of N-MoO_2 (208.7 mV dec^{-1}) and Co-MoO_2 (211.5 mV dec^{-1}) , indicating that the HER for Co-N-MoO_2 proceeded through a Volmer-Heyrovsky mechanism and the electrochemical desorption process was the rate-limiting step.

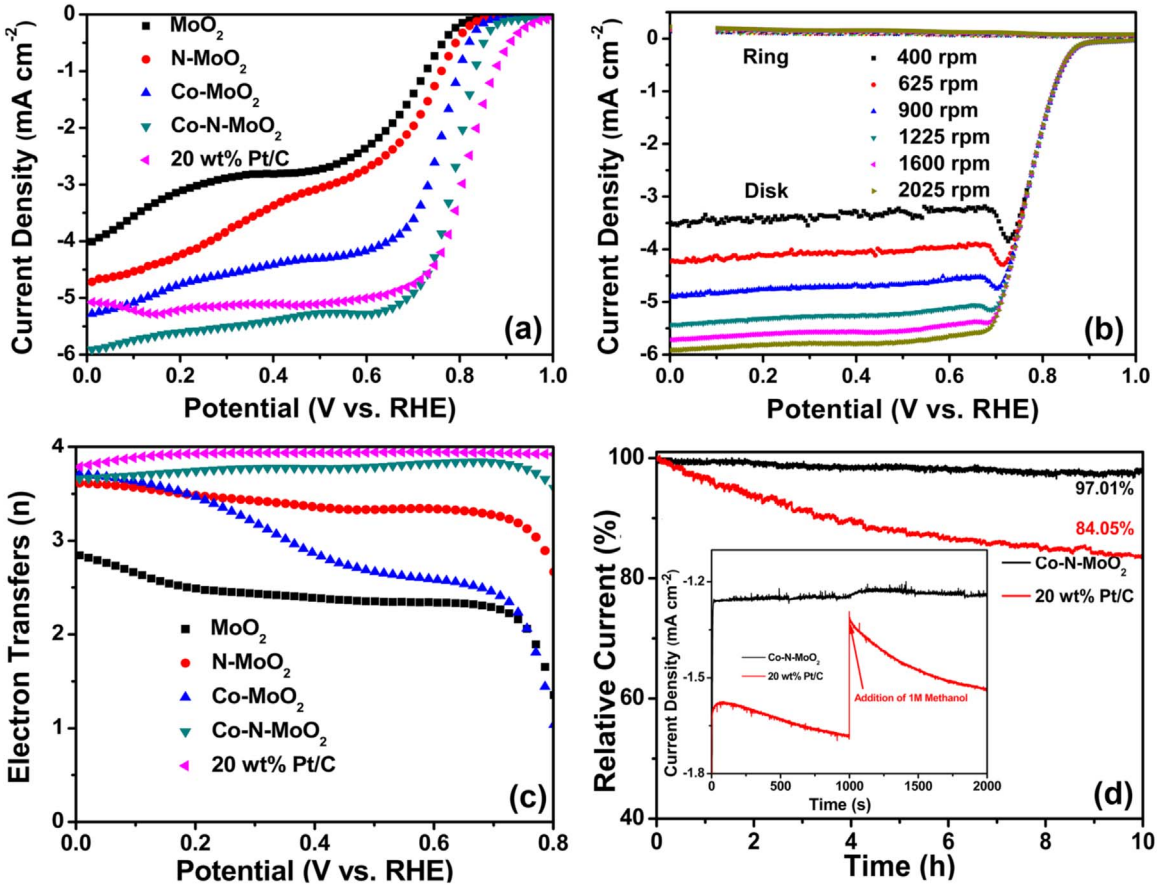

Fig. 3. (a) RRDE voltammograms of MoO_2, N-MoO_2, Co-MoO_2, Co-N-MoO_2 and 20 wt% Pt/C at a rotation rate of 1600 rpm and (b) RRDE voltammograms of Co-N-MoO_2 at different rotation rates with ring potential of +1.5 V in an O_2-saturated 0.1 M KOH solution at 10 mV s^{-1}. (c) Number of electron transfer of MoO_2, N-MoO_2, Co-MoO_2, Co-N-MoO_2 and 20 wt% Pt/C, as a function of electrode potential. (d) Chronoamperometric responses of Co-N-MoO_2 and 20 wt% Pt/C at +0.47 V vs. RHE (900 rpm) without and with 1 M methanol (inset).

Electrochemical impedance spectroscopy (EIS) was also used to investigate the electrode kinetics in HER. The comparison of Nyquist plots among Co-N-MoO_2-modified electrode and other control samples were shown in Fig. 4c. The decreasing charge-transfer resistance (Rct) value of Co-N-MoO_2-modified electrode (360.1 Ω) was smaller than those of MoO_2 (2675.3 Ω), N-MoO_2 (1570.0 Ω) and Co-MoO_2 (454.1 Ω) with an overpotential of 150 mV. Lower resistance suggested a faster reaction rate of HER, indicating that Co-N-MoO_2-modified electrode was more active than other samples. Besides, the electrical electronic conductivity (Rs) of electrodes that removed the influence of glassy carbon electrode (Fig. S11a) increased in order of Co-N-MoO_2 (7.3 Ω) < Co-MoO_2 (7.9 Ω) < N-MoO_2 (17.5 Ω) < MoO_2 (33.2 Ω), which implied that N-doped and Co-doped treatment reduced the electrical conduction resistance and leaded to the enhanced HER catalytic activity. The typical Nyquist plots of Co-N-MoO_2-modified electrode at various overpotentials were shown in Fig. S11b. It can be seen that the Rct values decreased apparently with the increased overpotentials, from 661.2 Ω at 80 mV to 360.1 Ω at 150 mV, suggesting the decreasing charge-transfer resistance (Rct) with the increased negative potentials.

The double-layer capacitance of Co-N-MoO_2 and other samples were measured by cyclic voltammograms (CVs), which was an important parameter to estimate the electrochemically active area at the solid-liquid interface. The CVs curves under various scan rates of different samples were shown in Fig. S12. The double-layer capacitance of Co-N-MoO_2 (16.5 mF cm^{-2}) was bigger than those of N-MoO_2 (8.9 mF cm^{-2}), Co-MoO_2 (6.1 mF cm^{-2}) and MoO_2 (3.4 mF cm^{-2}), as exhibited in Fig. 4d. The larger electrochemically active area was associated with more active sites on the surface of Co-N-MoO_2 at the solid-liquid interface, contributing to the excellent HER activity.

The durability was crucial aspects for HER catalysts, which was measured by accelerated degradation testing and chronopotentiometry at fixed potentials over extended periods in 0.1 M KOH. At an overpotential of 320 mV, the Co-N-MoO_2-modified electrode was operated continuously for 10 h and a little increase of current density was observed, suggesting the long-term extraordinary durability for HER in 0.1 M KOH (Fig. 4e). The polarization curves of Co-N-MoO_2 before and after i-t testing further confirmed robust stability with a slight increase in the current density (Fig. 4f). In addition, no significant changes of the morphology (inset of Fig. 4f) confirmed the structural integrity of Co-N-MoO_2 as well as catalytic stability.

Note that such an HER performance of Co-N-MoO_2 (onset potential of −69 mV vs. RHE, 258 mV at 10 mA cm^{-2}, and Tafel slope of 126.8 mV dec^{-1}) was markedly better than or comparable to those of the most active HER electrocatalysts in alkaline solutions, such as porous cobalt based thin film (−38 mV, 133 mV dec^{-1}) [42], compact MoO_2/Ni foam (124 mV, 116 mV dec^{-1}) [43], cobalt-carbon-nitrogen (−81 mV, 178 mV dec^{-1}) [44], cobalt-embedded nitrogen-rich carbon nanotubes (−160 mV,370 mV dec^{-1}) [24], cobalt-sulfide/fluorine-doped tin oxide (−100 mV) [45] (Table S3). The superior ORR and HER performance observed herein with Co-N-MoO_2 was attributed to the following aspects. Firstly, the one-dimensional structure of MoO_2 nanowires with high electrochemical area facilitated the diffusion among the electrocatalyst, electrolyte and gas [46,47]. Secondly, the good electrical conductivity of MoO_2 nanowires effectively collected and rapidly transferred electrons from the electrocatalysts to electrode [33]. Thirdly, the synergistic manipulation of N and Co doping with the opposite electron density states leaded to the relatively moderate bonding energy of Mo-H/O, and caused the enhanced catalytic activity with more catalytically active sites [31,48–50].

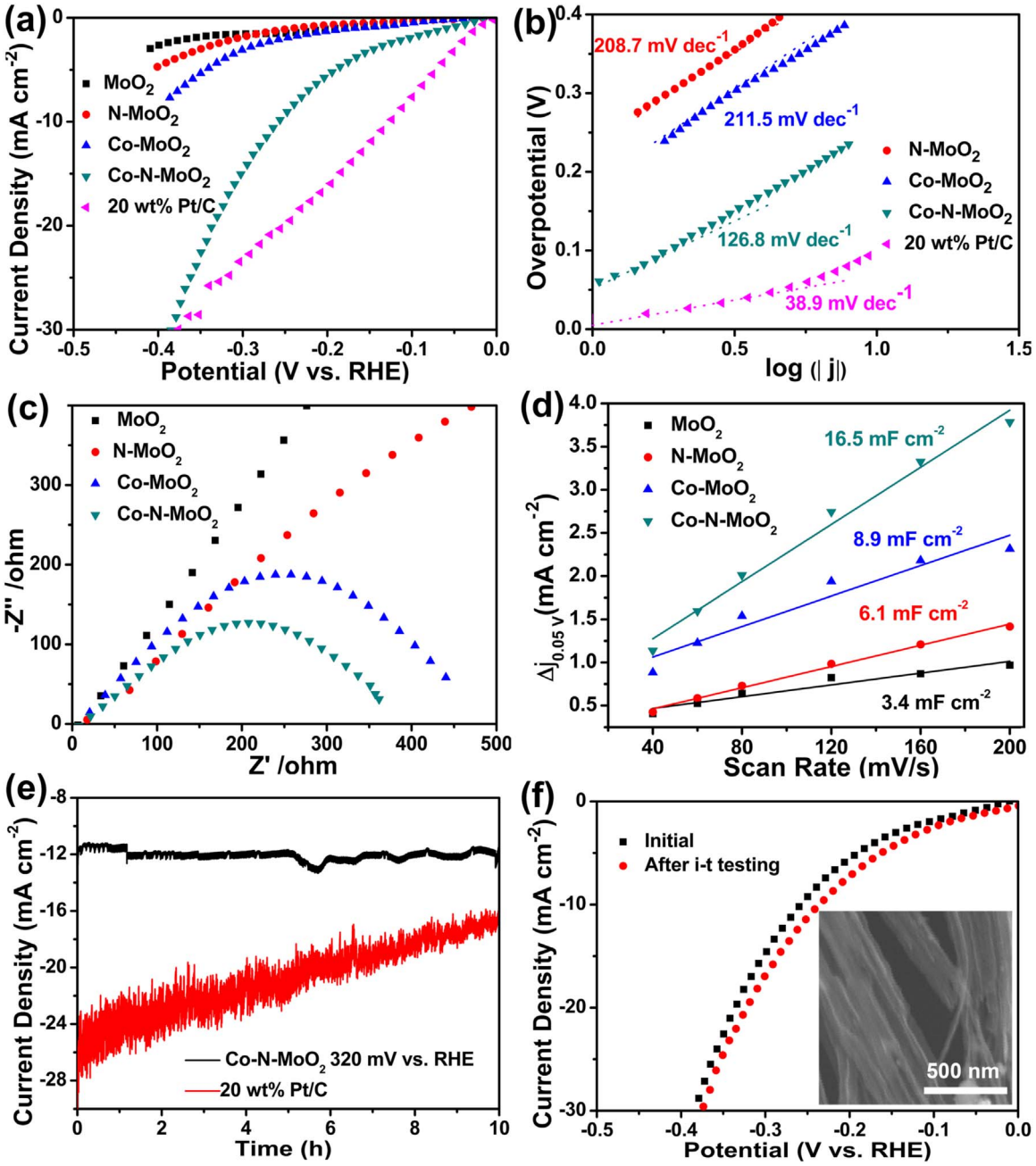

Fig. 4. (a) Polarization curves of MoO_2, N-MoO_2, Co-MoO_2, Co-N-MoO_2 and 20 wt% Pt/C with iR correction in 0.1 M KOH at scan rates of 2 mV s^{-1}. (b) Tafel plots derived from (a). (c) Nyquist plots of MoO_2, N-MoO_2, Co-MoO_2, Co-N-MoO_2 modified electrodes at 150 mV HER overpotentials in 0.1 M KOH. (d) The capacitive currents at +0.05 V vs. RHE as a function of scan rates for MoO_2, N-MoO_2, Co-MoO_2, Co-N-MoO_2 and 20 wt% Pt/C. (e) Chronoamperometric response for Co-N-MoO_2 and 20 wt% Pt/C at −320 mV vs. RHE for 10 h. (f) Polarization curves and SEM image (inset) of Co-N-MoO_2 before and after i-t testing.

4. Conclusions

In summary, we developed Co-N-doped MoO_2 nanowires catalysts by employing MoO_2 nanowire as templates and substrates. The XRD and XPS results confirmed the successful Co and N doping into MoO_2 nanowires. The most active Co-N-MoO_2 nanowire exhibited high ORR activity (an onset potential of +0.87 V vs. RHE), high selectivity (electron transfer number of 3.56–3.68), and excellent electrochemical stability. In addition, Co-N-MoO_2 as multifunctional catalysts also exhibited high HER performance of low onset potential (−69 mV vs. RHE) with Tafel slope of 126.8 mV dec^{-1}. The prominent HER performance with a low overpotential (69 mV vs. RHE), high electrochemical area and robust stability in 0.1 M KOH, are associated with the defined nanowire structures and homogeneous doping of Co/N into MoO_2 with numerous active sites. The concept of the one-dimensional conductive substrate with co-doping process demonstrated here is attractive for broad applications for heterogeneous catalysis.

Acknowledgements

We thank the Fundamental Research Funds for the Project of Public Interest Research and Capacity Building of Guangdong Province (2014A010106005), Guangdong Innovative and Entrepreneurial Research Team Program (2014ZT05N200), and the National Natural Science Foundation of China (51502096).

Appendix A. Supplementary material

Supplementary data associated with this article can be found in the online version at http://dx.doi.org/10.1016/j.nanoen.2017.03.032.

References

[1] Y. Kang, X. Ye, J. Chen, Y. Cai, R.E. Diaz, R.R. Adzic, E.A. Stach, C.B. Murray, J. Am. Chem. Soc. 135 (2013) 42–45.
[2] C. Zhang, S.Y. Hwang, A. Trout, Z. Peng, J. Am. Chem. Soc. 136 (2014) 7805–7808.
[3] W. Zhou, J. Jia, J. Lu, L. Yang, D. Hou, G. Li, S. Chen, Nano Energy (2016).
[4] K. Waki, R.A. Wong, H.S. Oktaviano, T. Fujio, T. Nagai, K. Kimoto, K. Yamada, Energy Environ. Sci. 7 (2014) 1950–1958.
[5] M. Zhou, H.-L. Wang, S. Guo, Chem. Soc. Rev. 45 (2016) 1273–1307.
[6] A. Qaseem, F. Chen, X. Wu, R.L. Johnston, Catal. Sci. Technol. 6 (2016) 3317–3340.
[7] D.-W. Wang, D. Su, Energy Environ. Sci. 7 (2014) 576–591.
[8] K. Zhou, W. Zhou, X. Liu, Y. Wang, J. Wan, S. Chen, ACS Appl. Mater. Interfaces 6 (2014) 14911–14918.
[9] J. Duan, S. Chen, M. Jaroniec, S.Z. Qiao, ACS Catal. 5 (2015) 5207–5234.
[10] J. Deng, P. Ren, D. Deng, X. Bao, Angew. Chem. Int. Ed. 54 (2015) 2100–2104.
[11] M. Zhou, C. Yang, K.-Y. Chan, Adv. Energy Mater. 4 (2014) 1400840.
[12] S. Chen, J. Duan, P. Bian, Y. Tang, R. Zheng, S.-Z. Qiao, Adv. Energy Mater. 5 (2015) 1500936.
[13] F. Cheng, Y. Su, J. Liang, Z. Tao, J. Chen, Chem. Mater. 22 (2010) 898–905.
[14] C. Zhang, M. Antonietti, T.-P. Fellinger, Adv. Funct. Mater. 24 (2014) 7655–7665.
[15] J. Duan, S. Chen, S. Dai, S.Z. Qiao, Adv. Funct. Mater. 24 (2014) 2072–2078.
[16] M. Li, X. Bo, Y. Zhang, C. Han, A. Nsabimana, L. Guo, J. Mater. Chem. A 2 (2014) 11672–11682.
[17] J. Duan, S. Chen, B.A. Chambers, G.G. Andersson, S.Z. Qiao, Adv. Mater. 27 (2015) 4234–4241.
[18] Y. Zhao, L. Kuai, Y. Liu, P. Wang, H. Arandiyan, S. Cao, J. Zhang, F. Li, Q. Wang, B. Geng, H. Sun, Sci. Rep. 5 (2015) 8722.
[19] Z. Yan, J. Xie, J. Jing, M. Zhang, W. Wei, S. Yin, Int, J. Hydrog. Energy 37 (2012) 15948–15955.
[20] Y. Jin, P.K. Shen, J. Mater. Chem. A 3 (2015) 20080–20085.
[21] Y. Jin, H. Wang, J. Li, X. Yue, Y. Han, P.K. Shen, Y. Cui, Adv. Mater. 28 (2016) 3785–3790.
[22] J. Liang, R.F. Zhou, X.M. Chen, Y.H. Tang, S.Z. Qiao, Adv. Mater. 26 (2014) 6074–6079.
[23] S. Guo, D. Li, H. Zhu, S. Zhang, N.M. Markovic, V.R. Stamenkovic, S. Sun, Angew. Chem. Int. Ed. 52 (2013) 3465–3468.
[24] X. Zou, X. Huang, A. Goswami, R. Silva, B.R. Sathe, E. Mikmeková, T. Asefa, Angew. Chem. 126 (2014) 4461–4465.
[25] H. Fei, J. Dong, M.J. Arellano-Jiménez, G. Ye, N.D. Kim, E.L. Samuel, Z. Peng, Z. Zhu, F. Qin, J. Bao, Nat. Commun. 6 (2015).
[26] W. Zhou, Y. Zhou, L. Yang, J. Huang, Y. Ke, K. Zhou, L. Li, S. Chen, J. Mater. Chem. A 3 (2015) 1915–1919.
[27] W. Zhou, J. Zhou, Y. Zhou, J. Lu, K. Zhou, L. Yang, Z. Tang, L. Li, S. Chen, Chem. Mater. 27 (2015) 2026–2032.
[28] Q. Gao, C. Zhang, S. Xie, W. Hua, Y. Zhang, N. Ren, H. Xu, Y. Tang, Chem. Mater. 21 (2009) 5560–5562.
[29] X. Liu, D. Wu, W. Ji, W. Hou, J. Mater. Chem. A 3 (2015) 968–972.
[30] C. Wan, B.M. Leonard, Chem. Mater. 27 (2015) 4281–4288.
[31] H. Lin, N. Liu, Z. Shi, Y. Guo, Y. Tang, Q. Gao, Adv. Funct. Mater. 26 (2016) 5590–5598.
[32] Y. Sun, X. Hu, W. Luo, Y. Huang, ACS Nano 5 (2011) 7100–7107.
[33] L. Yang, W. Zhou, D. Hou, K. Zhou, G. Li, Z. Tang, L. Li, S. Chen, Nanoscale 7 (2015) 5203–5208.
[34] J. Liu, S. Tang, Y. Lu, G. Cai, S. Liang, W. Wang, X. Chen, Energy Environ. Sci. 6 (2013) 2691–2697.
[35] W. Tang, C.X. Peng, C.T. Nai, J. Su, Y.P. Liu, M.V.V. Reddy, M. Lin, K.P. Loh, Small 11 (2015) 2446–2453.
[36] B. Cao, G.M. Veith, R.E. Diaz, J. Liu, E.A. Stach, R.R. Adzic, P.G. Khalifah, Angew. Chem. Int. Ed. 52 (2013) 10753–10757.
[37] F. Ronconi, M.P. Santoni, F. Nastasi, G. Bruno, R. Argazzi, S. Berardi, S. Caramori, C.A. Bignozzi, S. Campagna, Dalton Trans. 45 (2016) 14109–14123.
[38] Y. Liang, Y. Li, H. Wang, J. Zhou, J. Wang, T. Regier, H. Dai, Nat. Mater. 10 (2011) 780–786.
[39] S. Jiang, C. Zhu, S. Dong, J. Mater. Chem. A 1 (2013) 3593–3599.
[40] S. Chao, Q. Cui, K. Wang, Z. Bai, L. Yang, J. Qiao, J. Power Sources 288 (2015) 128–135.
[41] A. Wu, C. Tian, H. Yan, Y. Jiao, Q. Yan, G. Yang, H. Fu, Nanoscale 8 (2016) 11052–11059.
[42] Y. Yang, H. Fei, G. Ruan, J.M. Tour, Adv. Mater. 27 (2015) 3175–3180.
[43] Y. Jin, H. Wang, J. Li, X. Yue, Y. Han, P.K. Shen, Y. Cui, Adv. Mater. 28 (2016) 3785–3790.
[44] H. Jin, J. Wang, D. Su, Z. Wei, Z. Pang, Y. Wang, J. Am. Chem. Soc. 137 (2015) 2688–2694.
[45] Y. Sun, C. Liu, D.C. Grauer, J. Yano, J.R. Long, P. Yang, C.J. Chang, J. Am. Chem. Soc. 135 (2013) 17699–17702.
[46] L. Liao, S. Wang, J. Xiao, X. Bian, Y. Zhang, M.D. Scanlon, X. Hu, Y. Tang, B. Liu, H.H. Girault, Energy Environ. Sci. 7 (2014) 387–392.
[47] W. Zhou, X.-J. Wu, X. Cao, X. Huang, C. Tan, J. Tian, H. Liu, J. Wang, H. Zhang, Energy Environ. Sci. 6 (2013) 2921–2924.
[48] Y. Zheng, Y. Jiao, L.H. Li, T. Xing, Y. Chen, M. Jaroniec, S.Z. Qiao, ACS Nano 8 (2014) 5290–5296.
[49] H. Fei, J. Dong, M.J. Arellano-Jiménez, G. Ye, N. Dong Kim, E.L.G. Samuel, Z. Peng, Z. Zhu, F. Qin, J. Bao, M.J. Yacaman, P.M. Ajayan, D. Chen, J.M. Tour, Nat. Commun. 6 (2015) 8668.
[50] H.J. Qiu, Y. Ito, W. Cong, Y. Tan, P. Liu, A. Hirata, T. Fujita, Z. Tang, M. Chen, Angew. Chem. 127 (2015) 14237–14241.

Linjing Yang received B.S. degree from Hebei University of Technology in 2014. She is pursuing her M.D. degree under the supervision of Prof. Weijia Zhou and Prof. Shaowei Chen in New Energy Research Institute, South China University of Technology. Her research interests include electrocatalytic water splitting and oxygen reduction.

Jiayuan Yu obtained his B.S. Degree from School of Materials Science and Engineering, China University of Mining and Technology in 2011, and now is a master degree candidate at South China Normal University under the supervision of Dr. Benli Chu. He is doing research under the supervision of Prof. Weijia Zhou in New Energy Research Institute, South China university of Technology. His research interest mainly contains of design and synthesis catalysts for hydrogen evolution reaction, photocatalytic hydrogen evolution and electrochemical water treatment.

Zhaoqian Wei received B.S. degree from Guizhou University of Technology in 2016. She is pursuing her M.D. degree under the supervision of Prof. Weijia Zhou and Prof. Shaowei Chen in New Energy Research Institute, South China University of Technology (SCUT). Her research interests include electrocatalytic water splitting and CO_2 reduction.

Guixiang Li obtained his B.S. Degree from school of Environmental Science and Engineering, Kunming University of Science and Technology in 2016, and now is currently pursuing a Master under the supervision of Prof. Weijia Zhou in the school of Environment and Energy at South China University of Technology, China. His research is focused on the synthesis of nanomaterials as electrocatalyst for hydrogen evolution reaction and electrochemical water treatment.

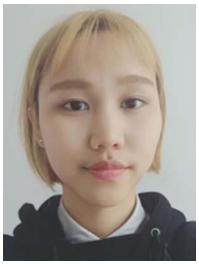

Lindie Cao has been studying in College of Environment and Energy, South China University of Technology (SCUT), since 2014. She is doing research under the supervision of Prof. Weijia Zhou in New Energy Research Institute. Her research interest is electro-catalytic water splitting.

Dr. Weijia Zhou completed his Ph.D. at Shandong University in 2012. He was doing research at Nanyang Technological University (NTU) in 2011. Now, Dr. Zhou is an associate professor in New Energy Research Institute, School of Environment and Energy, South China University of Technology (SCUT), China. His research interests are related to the design and synthesis of functional materials and devices for new energy conversion and storage, including photo and electro-catalytic water splitting, CO_2 reduction and supercapacitor.

Dr. Shaowei Chen obtained a B.Sc. degree from the University of Science and Technology of China, and then went to Cornell University receiving his M.Sc. and Ph.D. degrees in 1993 and 1996. Following a postdoctoral appointment in the University of North Carolina at Chapel Hill, he started his independent career in Southern Illinois University in 1998. In 2004, he moved to the University of California at Santa Cruz and is currently a Professor of Chemistry. He is also an adjunct professor at South China University of Technology. His research interest is primarily in the electron transfer chemistry of nanoparticle materials.